Journal of Asian Ceramic Societies 2 (2014) 102–116

Contents lists available at ScienceDirect

Journal of Asian Ceramic Societies

journal homepage: www.elsevier.com/locate/jascer

Design and optimization of coating structure for the thermal barrier coatings fabricated by atmospheric plasma spraying via finite element method

L. Wang[a,b,*], X.H. Zhong[a,b], Y.X. Zhao[a,b,c], S.Y. Tao[a,b], W. Zhang[b,d], Y. Wang[e], X.G. Sun[e]

[a] Key Laboratory of Inorganic Coating Materials, Chinese Academy of Sciences, Shanghai 200050, PR China
[b] Shanghai Institute of Ceramics, Chinese Academy of Sciences, Shanghai 200050, PR China
[c] University of Chinese Academy of Sciences, Beijing 100039, PR China
[d] State Key Laboratory of High Performance Ceramics and Superfine Microstructure, Shanghai Institute of Ceramics, Chinese Academy of Sciences, Shanghai 200050, PR China
[e] Laboratory of Nano Surface Engineering, School of Materials Science and Engineering, Harbin Institute of Technology, Harbin 150001, PR China

ARTICLE INFO

Article history:
Received 4 December 2013
Received in revised form 15 January 2014
Accepted 17 January 2014
Available online 20 February 2014

Keywords:
Thermal barrier coatings
Residual stress
Thermal insulation
Finite element simulation
Design and optimization

ABSTRACT

The first prerequisite for fabricating the thermal barrier coatings (TBCs) with excellent performance is to find an optimized coating structure with high thermal insulation effect and low residual stress. This paper discusses the design and optimization of a suitable coating structure for the TBCs prepared by atmospheric plasma spraying (APS) using the finite element method. The design and optimization processes comply with the rules step by step, as the structure develops from a simple to a complex one. The research results indicate that the suitable thicknesses of the bond-coating and top-coating are 60–120 μm and 300–420 μm, respectively, for the single ceramic layer YSZ/NiCoCrAlY APS-TBC. The embedded interlayer (50 wt.%YSZ + 50 wt.%NiCoCrAlY) will further reduce the residual stress without sacrificing the thermal insulation effect. The double ceramic layer was further considered which was based on the single ceramic layer TBC. The embedded interlayer and the upper additional ceramic layer will have a best match between the low residual stress and high thermal insulation effect. Finally, the optimized coating structure was obtained, i.e., the $La_2Ce_2O_7$(LC)/YSZ/Interlayer/NiCoCrAlY coating structure with appropriate layer thickness is the best choice. The effective thermal conductivity of this optimized LC/YSZ/IL/BL TBC is 13.2% lower than that of the typical single ceramic layer YSZ/BL TBC.

1. Introduction

With the development of the modern aerospace technology, the demand for the efficiency of hot section components (e.g., vanes or blades) of advanced turbine and engine is becoming higher and higher. The thermal barrier coatings (TBCs) on these hot section components are very important ceramic coating materials. They play an increasing role in improving the heat efficiency and thrust weight ratio of the turbine and engine [1–7]. Generally, the typical TBCs are composed of double layers, i.e., metallic layer and ceramic layer. The metallic layer is often MCrAlY (here M = Ni and/or Co), which is deposited between the super-alloy substrates and the ceramic layer in order to relieve the thermal mismatch between them. The ceramic layer is usually composed of 8 wt.% (4.5 mol.%) yttria-stabilized zirconia or other zirconate (aluminate)-based $A_xB_yO_7$ (where A denotes the rare-earth element and B denotes Zr, Ce or Al). It often impedes the high-velocity heat flux by impacting it directly onto the superalloy substrates. Atmospheric plasma spraying (APS) is one of the most important techniques to fabricate the TBCs and it is widely used in actual application [8–15].

The low residual stress and high thermal insulation effect are the two primary factors to evaluate the TBCs. The low residual stress will ensure that the reliability and durability are high enough. The coating has a long lifetime when it is used in the actual hot section components, especially when the TBCs are subjected to severe exterior environment. The high thermal insulation effect can make sure that the hot section components can be used at higher temperatures, and this will further improve the heat efficiency and thrust weight ratio of the turbine and engine [16–19]. In fact, many factors can affect the magnitude and distribution of the residual

* Corresponding author at: Key Laboratory of Inorganic Coating Materials, Chinese Academy of Sciences, Shanghai 200050, PR China. Tel.: +86 021 69906320; fax: +86 021 69906322.
E-mail addresses: glacier_hit@126.com, L.Wang@mail.sic.ac.cn (L. Wang).

Peer review under responsibility of The Ceramic Society of Japan and the Korean Ceramic Society.

Production and hosting by Elsevier

2187-0764 Crown Copyright © 2014 Production and hosting by Elsevier B.V. on behalf of The Ceramic Society of Japan and the Korean Ceramic Society. All rights reserved.
http://dx.doi.org/10.1016/j.jascer.2014.01.006

stress in the TBCs, such as defects (cracks and pores) in the ceramic layer, oxide thickness, interlayer, interface asperity, exterior environment (temperature, thermal flux, radiation, impact load) and so on [20–25]. In fact, the coating thickness plays an important role in controlling the stress distribution and magnitude of the as-sprayed TBCs. The coating thickness also plays a key role in controlling the thermal insulation effect of the as-sprayed TBCs. Generally, the thermal insulation effect will increase with the increase in ceramic layer thickness [26–28]. But the residual stress will also increase with the increase in ceramic layer thickness [29,30]. Many previous literatures have testified this viewpoint. Besides the thick thermal barrier coatings (TTBCs) with the segmentation cracks prepared under special processing condition, spallation can also be induced in the TBCs and the coating can be separated from the substrate directly when the ceramic layer thickness exceeds a certain value [31,32]. Therefore obtaining an optimized coating structure with high thermal insulation effect and low residual stress is the first prerequisite for fabricating the TBCs with excellent performance. This will be a very challenging and interesting topic.

Previous work often focused on thermal insulation and residual stress based on some specified coating models independently, but without much importance to the optimization of the coating structure with regard to the two factors [33–35]. The objective of the current work is to design and optimize the coating structure of the TBCs with excellent match between the high thermal insulation effect and low residual stress. And the design and optimization results will provide a powerful guide to fabricate the TBCs with excellent performance.

2. Design and optimization process

The design and optimization process based on the finite element simulation will be described in detail in this section. The finite element simulation procedure mainly includes establishing the designed model, applying the proper boundary and initial conditions, setting suitable solution methods and steps, and solving the designed model. The final goal of the optimization process is to find the suitable coating structure model and coating thickness by comparing the lowest residual stress and highest thermal insulation effect. And we sincerely hope that the design and the optimization results will provide a powerful guide to prepare the APS-TBC with excellent performance eventually.

2.1. Sources of the residual stress in the TBCs

The design and optimization processes are based on the finite element simulation procedure, so this procedure is the most important step to realize the goal of the design and optimization. As the thermal insulation effect of the TBCs mainly depends on the thickness of the ceramic layer, calculation of the residual stress will be more complicated compared with that of the thermal insulation effect; hence the finite element simulation of residual stress is preformed first. Usually, the residual stress in the TBCs after thermal spraying often includes the following three parts: quenching stress (σ_q), thermal mismatch stress (σ_t) and phase transformation stress (σ_p). So the total residual stress (σ) can be written as follows:

$$\sigma = \sigma_q + \sigma_t + \sigma_p \tag{1}$$

The quenching stress σ_q can be defined as that which can be induced in the ceramic coating when the coating is sprayed or deposited onto the cooler substrate or the former deposited splats. Analytically, the magnitude of the induced tensile quenching stress in the process of plasma spraying can be estimated from [36–38]:

$$\sigma_q = \alpha_c(T_m - T_s)E_c \tag{2}$$

where α_c and E_c are the coefficient of thermal expansion (CTE) of coating and the elastic modulus of coating, respectively. T_m is the temperature where stress relaxation by plastic flow or plastic deformation is inhibited. As the droplet usually exhibits a semi-molten state, the spray temperature is usually below T_m. T_s is the substrate temperature. The thermal mismatch stress was usually generated by the CTE mismatch between the ceramic layer and the substrate/metallic layer during the cooling of the entire coating system (including the substrate) from the spraying state to the ambient temperature. In the two-dimensional analysis, the thermal mismatch stress generated in the TBC can be calculated as:

$$\sigma_t = \frac{E_c}{1-\nu_c}\Delta\alpha\,\Delta T = \frac{E_c}{1-\nu_c}(\alpha_c - \alpha_s)(T - T_0) \tag{3}$$

where $\Delta\alpha$, ΔT and ν_c are the CTE difference between the substrate and coating, the temperature difference upon cooling and the Poisson's ratio of coating, respectively. α_c and α_s are the thermal conductivities of the ceramic layer and the substrate, respectively. T is the temperature of the spray state; T_0 is the ambient temperature. The phase transformation-induced stress was usually generated in the process of the solidification of liquid particles or solid-state transformation during plasma spraying. The induced stress in the process of solidification of liquid feedstock particles could be relaxed by the presence of liquid phase in the process of thermal spraying. Also, the addition of 8 wt.% (4.5 mol%) Y_2O_3 into ZrO_2 can inhibit the phase transformation of ZrO_2 from tetragonal phase to monoclinic phase. Consequently, the phase transformation-induced stress in the plasma sprayed 8YSZ TBC can be ignorable. In fact, as for the pure ZrO_2 coating, it can be seen from the phase diagram of ZrO_2 and Y_2O_3 binary system (Fig. 1), the transformation from tetragonal (T) to monoclinic (M) phase can occur. This type of transformation can lead to a relatively higher volume expansion (3–5%) which can produce inner stress in the coating. This type of phase transformation can be partially prevented by the addition of Y_2O_3 into the ZrO_2 and its subsequent solid-solution treatment in the ZrO_2 crystal lattice [39–42]. So in the current work, the phase transformation was ignored, and the residual stress was composed of thermal mismatch stress and quenching stress. The phase transformation can be regarded as a portion of residual stress but was ignored, which can be also seen in other references [43,44].

According to the above description, the overall magnitude of residual stress induced in plasma sprayed coatings in the process of plasma spraying is the summation of quenching stress σ_q and thermal mismatch stress σ_t, i.e.

$$\sigma = \alpha_c(T_m - T_s)E_c + \frac{E_c}{1-\nu_c}(\alpha_c - \alpha_s)(T - T_0) \tag{4}$$

2.2. Finite element simulation procedure

In the current work, a circular disk specimen is considered, and the problem can be reduced to a two-dimensional axisymmetric case in the radial and through-thickness direction as schematically shown in Fig. 2. In order to simplify the writing and expression, the bond-coat layer, interlayer, YSZ layer and $La_2Ce_2O_7$ layer were denoted as BL, IL, YSZ and LC, respectively. Three types of models have been established, i.e., YSZ/BL, YSZ/IL/BL and LC/YSZ/IL/BL. The thickness of the substrate, NiCoCrAlY metallic layer, Interlayer (50 wt.%NiCoCrAlY + 50 wt.%YSZ), YSZ ceramic layer and LC ceramic layer is defined as t_s, t_b, t_i, t_y and t_l, respectively, and the five optimization parameters $n_1 = t_b/t_s$, $n_2 = t_i/t_s$, $n_3 = t_y/t_s$, $n_4 = t_l/t_s$ and $m = n_4/n_3$ have been used in our calculation process. The property parameters used in the finite element simulation are listed in Table 1 [45–51].

The finite element simulation was based on the following assumptions: (1) All layers are homogeneous and isotropic, there

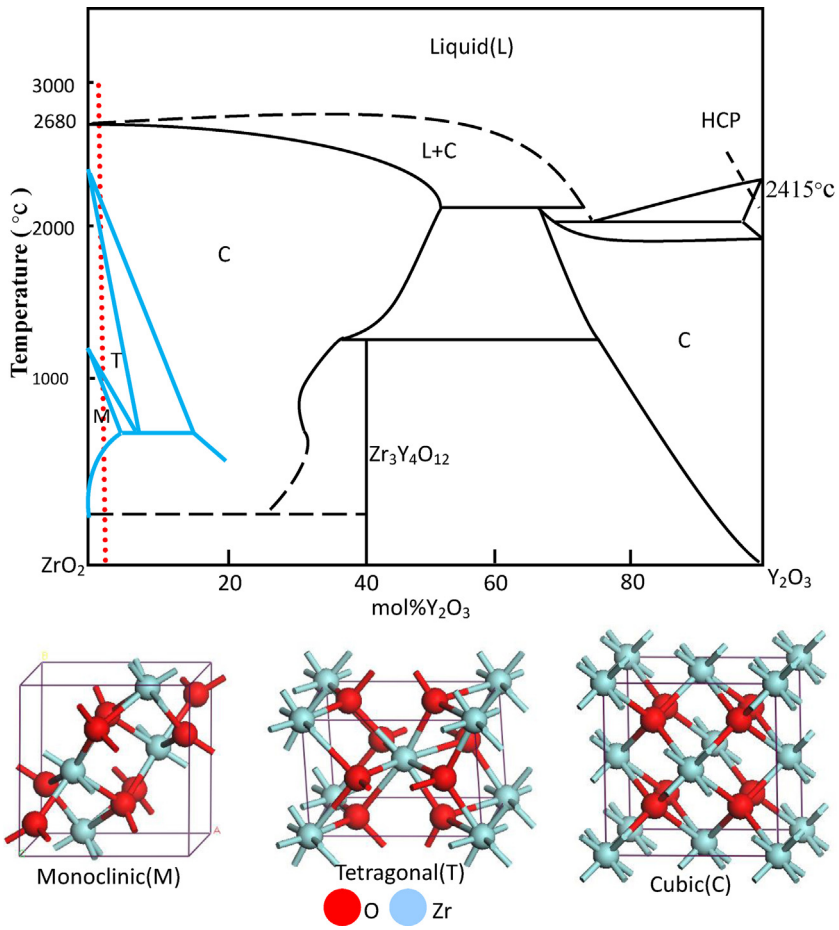

Fig. 1. Phase diagram of ZrO_2 and Y_2O_3 binary system [39–42] (a) and schematic illustration of three types of ZrO_2 crystal structures (b).

are no defects in each layer, and the interfaces between the two adjacent layers are flat without defects or wave characteristic; but these will be further investigated in our future work. (2) The upper surface of the top coat transfers heat with air by convection, the side surface is adiabatic, and heat radiation was not considered in the current simulation. (3) The creep and plastic deformation of all layers are negligible and were not taken into account. (4) The ceramic layer was assumed to be linear elastic; only when the stress is beyond the yield stress, crack can be initiated in the coating, and the coating begins to fail. The finite element simulation was performed using the commercial finite element software ANSYS (version 14.5) affiliated with APDL code. An axial symmetric problem was chosen in order to reduce the data processing time and to improve the computational efficiency. The Plane 13 element (four-node thermal-structure couple element) was selected in the current simulation work [52]. The meshes in the zone near the interface of the adjacent layers were refined to improve the accuracy of the calculation (Fig. 3). Constraints were imposed on the axial line and bottom side of the analyzed model, which can be viewed as the geometric boundary conditions. The coating was sprayed onto the cyclic-like

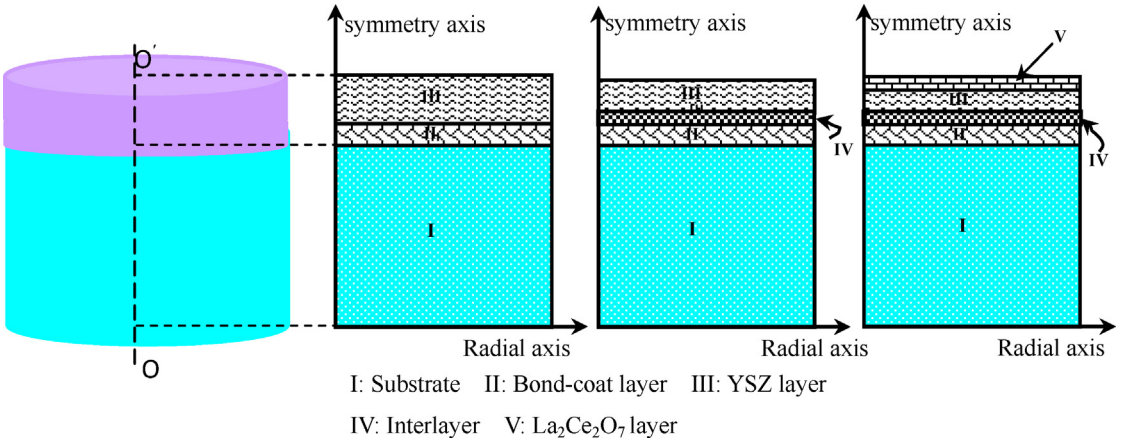

Fig. 2. Designed model used in the finite element simulation.

Table 1
Property parameters used in the finite element simulation [45–51].

Material	T (°C)	E (GPa)	ρ (kg/m^3)	α (10^{-6}/K)	ν	k (W/m K)	C (J/kg K)
$La_2Ce_2O_7$	25	49	7100	6.7	0.24	1.12	494
	400	44	7100	8.9	0.24	0.93	565
	800	38	7100	13.7	0.24	0.90	607
YSZ	25	53	4400	7.2	0.25	1.5	500
	400	52	4400	9.4	0.25	1.2	576
	800	46	4400	16	0.25	1.2	637
50%NiCoCrAlY + 50%YSZ	25	156	5860	11	0.275	3.1	517
	400	146	5860	19	0.275	3.8	621
	800	89	5860	35	0.275	5.6	689
NiCoCrAlY	25	225	7320	14	0.3	4.3	501
	400	186	7320	24	0.3	6.4	592
	800	147	7320	47	0.3	10.2	781
Ni-alloy substrate	25	200	8220	14.4	0.3	11.5	431
	400	179	8220	14.4	0.3	17.5	524
	800	149	8220	14.4	0.3	23.8	627

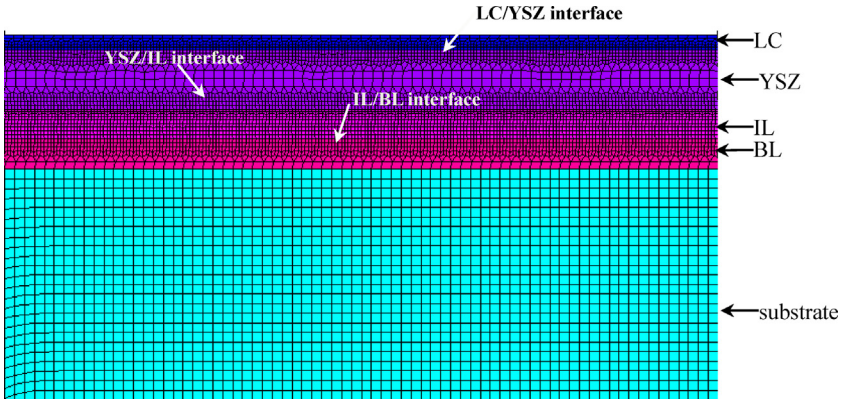

Fig. 3. Partial amplified mesh used in the finite element simulation of the LC/YSZ/IL/BL TBC.

substrates measuring Φ25 mm × 6 mm. The designed thickness of each layer was controlled at a suitable level. Selection of the initial and reference temperature is also very important in the process of finite element simulation. Generally, the material will melt when the temperature reaches the melting point of the material. It will exhibit liquid characteristic, and all parts of the material are relaxed and the stress is free. So the melting point can be defined as the reference temperature. In the current model, the initial and reference temperatures were set at 475 °C [53–56], 1680 °C, 1200 °C, 2100 °C and 2300 °C for substrate, bond coating, Interlayer, 8YSZ layer and LC layer, respectively. The temperature of the atmosphere was set at 27 °C, and the cooling time was assumed to be 1200 s, when the whole coating system reached the heat equilibrium state. The calculated residual stress in the current work includes both quenching stress σ_q and thermal mismatch stress σ_i. In addition, the heat transfer that is attributed to the convection between the plasma jet and the superalloy substrate was also included in the current model. The convective coefficient between the outer surfaces of the coating samples and the static air was assumed to be 100 W/(m^2 K).

2.3. Design and optimization process

The optimization process can be performed step by step complying with the rules, from a simple case to a complicated case. On the one hand, the design and optimization processes from the aspect of residual stress were performed. The design concept of the optimized coating structure from the aspect of gradual change of thermal expansion coefficients of the adjacent layers can be seen in Fig. 4. One of the most important aspects of the residual stress is the thermal mismatch stress induced due to the mismatch of

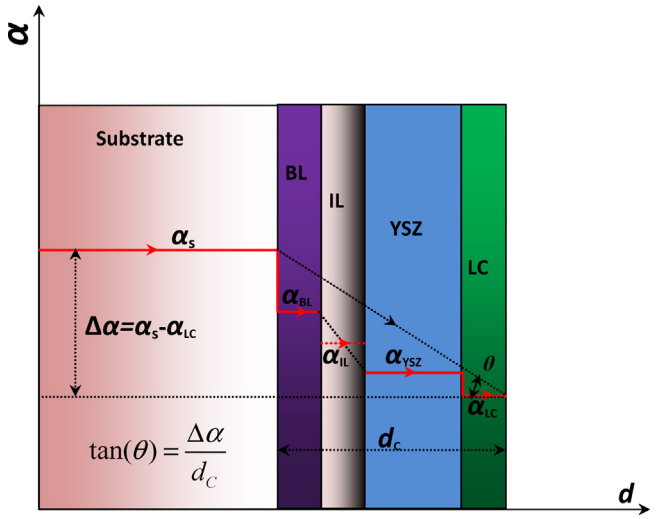

Fig. 4. Schematic illustration of the design concept of the optimized coating structure from the aspect of gradual change in thermal expansion coefficients of the adjacent layers.

the CTE between the adjacent layers. The basic design concept is to ensure that the CTE changes gradually along the through-thickness direction in the thermal barrier coating system in order to reduce the thermal mismatch stress and acquire the optimized coating structure. The low tan(θ) will guarantee the low residual stress. The bond-coat layer near the substrate usually has a relatively high thermal expansion coefficient, so it was usually deposited onto the substrate first. The interlayer was embedded between the bond-coat layer and the YSZ layer in order to reduce the thermal mismatch the two layers. The LC layer was deposited onto the surface of the YSZ layer for two reasons: (1) to improve the thermal insulation effect without increasing the residual stress of the whole coating system, and (2) to protect the YSZ layer from enduring higher temperature, as the thermal expansion coefficient of the LC layer is usually lower than that of the YSZ layer, and the LC layer is non-oxygen transparent and has lower thermal conductivity compared with the YSZ layer.

Firstly, as for the single ceramic layer YSZ/BL TBC, the two optimization parameters n_1 and n_2 were used in our calculation process. When the double layer TBCs model is considered, the minimum values of the radial stress (σ_{xx}), axial stress (σ_{yy}) and shear stress (σ_{xy}) are the function of t_s, n_1 and n_2. When the suitable t_s, n_1 and n_2 are obtained, it can be realized that σ_{xx}, σ_{yy} and σ_{xy} have the minimum values simultaneously, i.e., the optimization goal is to satisfy the following expressions:

$$\left.\begin{aligned}\min(\sigma_{xx}) &= f(t_s, n_1, n_2)\\ \min(\sigma_{yy}) &= f(t_s, n_1, n_2)\\ \min(\sigma_{xy}) &= f(t_s, n_1, n_2)\end{aligned}\right\} \quad (5)$$

Secondly, the embedded interlayer (50 wt.%YSZ + 50 wt.%NiCoCrAlY) was introduced in the TBC system. Based on the previous design and optimization results, the thickness of the interlayer was defined as t_i, and the thickness ratio between the interlayer and the substrate was defined as $n_3 = t_i/t_s$. In the triplex layer TBCs model, wherein the interlayer was embedded between the bond-coat layer and the YSZ layer, the minimum values of the radial stress (σ_{xx}), axial stress (σ_{yy}) and shear stress (σ_{xy}) are also the function of t_s, n_1, n_2 and n_3. When suitable t_s, n_1, n_2 and n_3 are obtained, it can be realized that σ_{xx}, σ_{yy} and σ_{xy} have the minimum values simultaneously, i.e., the optimization goal was to satisfy the following expressions:

$$\left.\begin{aligned}\min(\sigma_{xx}) &= g(t_s, n_1, n_2, n_3)\\ \min(\sigma_{yy}) &= g(t_s, n_1, n_2, n_3)\\ \min(\sigma_{xy}) &= g(t_s, n_1, n_2, n_3)\end{aligned}\right\} \quad (6)$$

Thirdly, the zirconate (aluminate)-based layer was further introduced in the TBC system based on the former design and optimization results. Here the $La_2Ce_2O_7$ (LC) was taken as the research object. The total thickness of the LC layer and YSZ layer was equal to that of the optimized YSZ layer thickness in the single ceramic layer YSZ/NiCoCrAlY TBC. Here the thickness ratio between LC and YSZ was defined as $m = t_l/t_y$. In the double ceramic layer TBCs model, i.e., the interlayer embedded between the bond-coat layer and the YSZ layer, the LC layer was deposited onto the surface of the YSZ layer, and the total thickness of the two adjacent ceramic layers (YSZ layer and LC layer) has a constant value. The minimum values of the radial stress (σ_{xx}), axial stress (σ_{yy}) and shear stress (σ_{xy}) are also the function of t_s, n_1, n_2, n_3 and m, and when the suitable t_s, n_1, n_2, n_3 and m values are obtained, it can be realized that σ_{xx}, σ_{yy} and σ_{xy} have the minimum values simultaneously, i.e., the optimization goal is to satisfy the following expressions:

$$\left.\begin{aligned}t_c = t_l + t_y &= \text{constant}\\ \min(\sigma_{xx}) &= g(t_s, n_1, n_2, n_3, m)\\ \min(\sigma_{yy}) &= g(t_s, n_1, n_2, n_3, m)\\ \min(\sigma_{xy}) &= g(t_s, n_1, n_2, n_3, m)\end{aligned}\right\} \quad (7)$$

On the other hand, the thermal insulation was also considered based on the design and optimization results of the coating structure from the aspect of residual stress. According to the basic theory of thermal transfer – Fourier's second law – in three-dimensional direction, the heat conduction equation can be expressed as:

$$\frac{\partial}{\partial x}\left(k_x\frac{\partial T}{\partial x}\right) + \frac{\partial}{\partial y}\left(k_y\frac{\partial T}{\partial y}\right) + \frac{\partial}{\partial z}\left(k_z\frac{\partial T}{\partial z}\right) + q_v = \frac{\partial}{\partial t}(\rho c T) \quad (8)$$

where T is the transient temperature, t is the time, ρ is the density, and k_x, k_y, k_z are thermal conductivities in x, y and z direction, respectively. C is the heat capacity, and q_v is the intensity of the internal heat source in the corresponding space.

As for the process of fabrication and cooling of plasma sprayed coating, the intensity of the internal heat source, i.e., q_v, is equal to zero. And only the heat conduction in the through-thickness direction (spray direction) was considered, so the above equation can be simplified as follows [57]:

$$\frac{\partial T}{\partial t} = \frac{k}{\rho C_p}\frac{\partial^2 T}{\partial y^2} \quad (9)$$

When the left and right boundaries of the coating model are considered to be adiabatic, i.e., $dT/dn = 0$, the effective thermal conductivity in the through-thickness direction (spray direction) can be calculated from [58]:

$$k_{eff} = \frac{h}{\Delta T W}\int_{\tau_{bot}} k(n\nabla T)d\tau \quad (10)$$

where h *and* W are the average thickness and the width of the coating model, respectively, ΔT is the temperature difference between the top side and bottom side of the coating model, and τ_{bot} is the lower horizontal boundary of the coating model with normal vector n. It can be further seen that the effective thermal conductivity k_{eff} is inversely proportional to the temperature difference ΔT according to the formula (10). The detailed calculation procedure of the effective thermal conductivity can be seen in our previous published paper [59,60].

Based on the optimization results from the aspect of residual stress, the low effective thermal conductivity of the whole coating system was further considered, i.e., the effective thermal conductivity is also the function of t_s, n_1, n_2, n_3 and m, the joint optimization was performed and the final optimization goal realized. The optimized coating structure of APS-TBCs when considering the residual stress level and the effective thermal conductivity simultaneously can be further expressed as follows:

$$\left.\begin{aligned}t_c = t_l + t_y &= \text{constant}\\ \min(\sigma_{xx}) &= g(t_s, n_1, n_2, n_3, m)\\ \min(\sigma_{yy}) &= g(t_s, n_1, n_2, n_3, m)\\ \min(\sigma_{xy}) &= g(t_s, n_1, n_2, n_3, m)\\ \min(k) &= g(t_s, n_1, n_2, n_3, m)\end{aligned}\right\} \quad (11)$$

The detailed process of the design and optimization of the coating structure for the APS-TBC is shown in Fig. 5. It must be

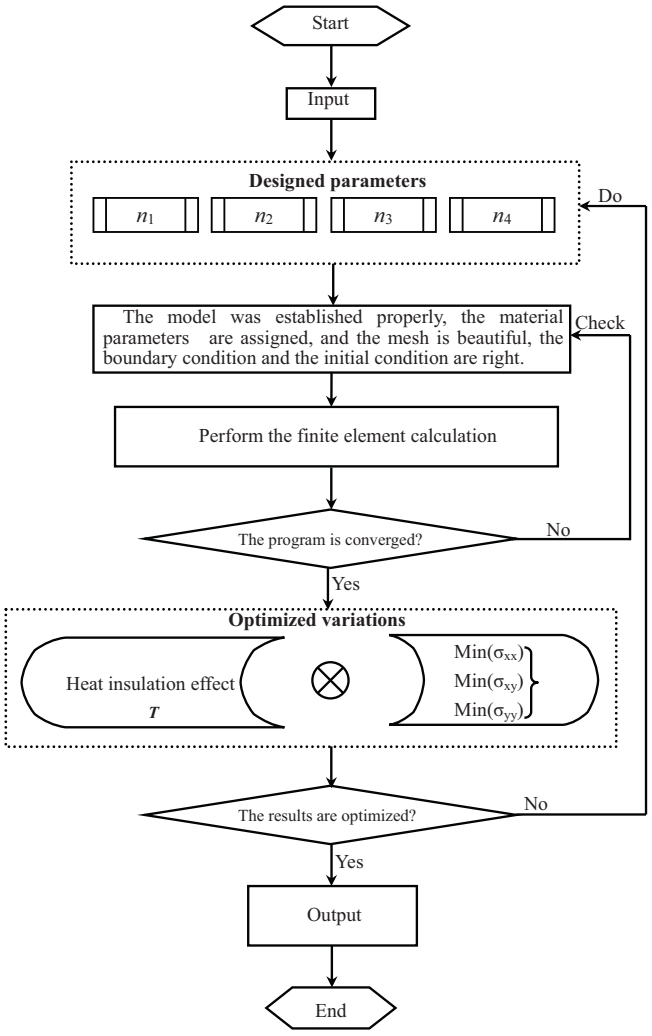

Fig. 5. Flow chart of the process of design and optimization of the coating structure.

specifically pointed out that all the processes of design and optimization are based on the finite element simulation. The thermal insulation effect and residual stress have been considered simultaneously.

2.4. Experimental procedure

In order to validate our current finite element simulation and optimization results, some necessary experiments were executed in the current work. The YSZ coatings, which used YSZ powder (Metco 204NS) as the feedstock, were fabricated by APS. Before spraying, the superalloy (GH3128) substrates were immersed in ethanol for ultrasonic cleaning for a dwell time of 15 min. After removal from ethanol, the substrates were then degreased and grit-blasted with 24-mesh brown corundum in order to enhance the mechanical interlocking between the layers and increase the bonding strength of the as-sprayed coatings. The feedstock was dried in an oven at 120 °C for 2 h, and particles of less than 200 mesh size were collected as the thermal sprayed feedstock. Then NiCoCrAlY, 8YSZ coatings were deposited onto the superalloy substrates in turn and the as-sprayed TBCs were fabricated. The feedstock was thermally sprayed using an Ar/H_2 APS torch (9 MB plasma gun, GH nozzle, Sulzer Metco, Westbury, NY, USA). The feedstock that was used to deposit the coatings was given externally. Detailed thermal spray parameters are presented in Table 2.

Table 2
Parameters used in plasma spraying.

Parameter	NiCoCrAlY	ZrO_2–8%Y_2O_3
Current (A)	530	570
Voltage (V)	53	55
Flow rate of primary gas (SCFH[a])	120	100
Feedstock giving rate (g/min)	5.0	6.8
Spray distance (mm)	110	80
Spray angle (°)	90	90
Spray velocity (mm/s)	30	30

[a] 1SCFH = 0.472 L min^{-1}.

Thermal shock resistance test was performed by using heating and water-quenching method. The coatings were deposited onto the cylinder-like superalloy substrates of size Φ25 mm × 6 mm.The samples were heated to 1150 °C with a dwell time of 5 min in a high temperature muffle furnace and then quickly thrown into water of temperature 20 °C. After the coating samples were cooled to the ambient temperature, they were taken out, dried and put in the high temperature muffle furnace again, and the same process repeated. The thermal cycle number when nearly 20% coating surface was destroyed (cracking and peeling are visible to the naked eye) was recorded as the thermal cycling lifetime of the as-sprayed coating. The dynamic macro-images of the destroyed coating samples were captured timely by a digital camera. The cross-section and the fracture surface were examined by using a scanning electron microscope (SEM, S-570, Hitachi, Tokyo, Japan).

3. Results and discussion

In this section, the design and optimization results of the coating structures based on the finite element simulation have been presented. The simulation results about the residual stress of different coating structures for the TBCs were extracted from the ANSYS visualization and analyzed systematically. Residual stress in the following three directions was obtained: the residual stress along the radial direction can be defined as radial stress (σ_{xx}). The residual stress that refers to stress profile through the thickness of the coatings can be defined as axial stress (σ_{yy}), and the residual stress that acts along the tangential direction can be defined as shear stress (σ_{xy}). The calculation and optimization of thermal insulation of several coating structures were further performed based on the finished optimization results of residual stress.

3.1. Design and optimization of YSZ/BL TBC

Fig. 6 shows the calculated residual stress along the YSZ/BL interface. The radial stress exhibited an increasing tendency along the YSZ/BL interface (radial direction). The maximum radial stress was located near the BL/YSZ interface and in the BL layer. It can be further seen that the radial stress also increases with increasing n_2. This indicates that when the thickness of the bond-coat layer is the same, the radial stress will increase with the thickness of the YSZ ceramic layer (Fig. 6a). From Fig. 6b, it can be seen that the maximum axial stress is located at the outer edge and in the BL layer, the axial stress nearly remains zero from the center line to the position near the edge along the YSZ/BL interface (radial direction), and then the stress increases and the maximum compressive stress occurs at the outer edge. It can be further seen that the maximum stress increases with increasing n_2 (i.e., increasing the thickness of the YSZ ceramic layer). The maximum shear stress is located at the BL/YSZ interface, and the board zone of the maximum shear stress is located at the YSZ layer. The shear stress also nearly remains zero from the center line to the position near the edge along the YSZ/BL interface (radial direction), and then the stress increases

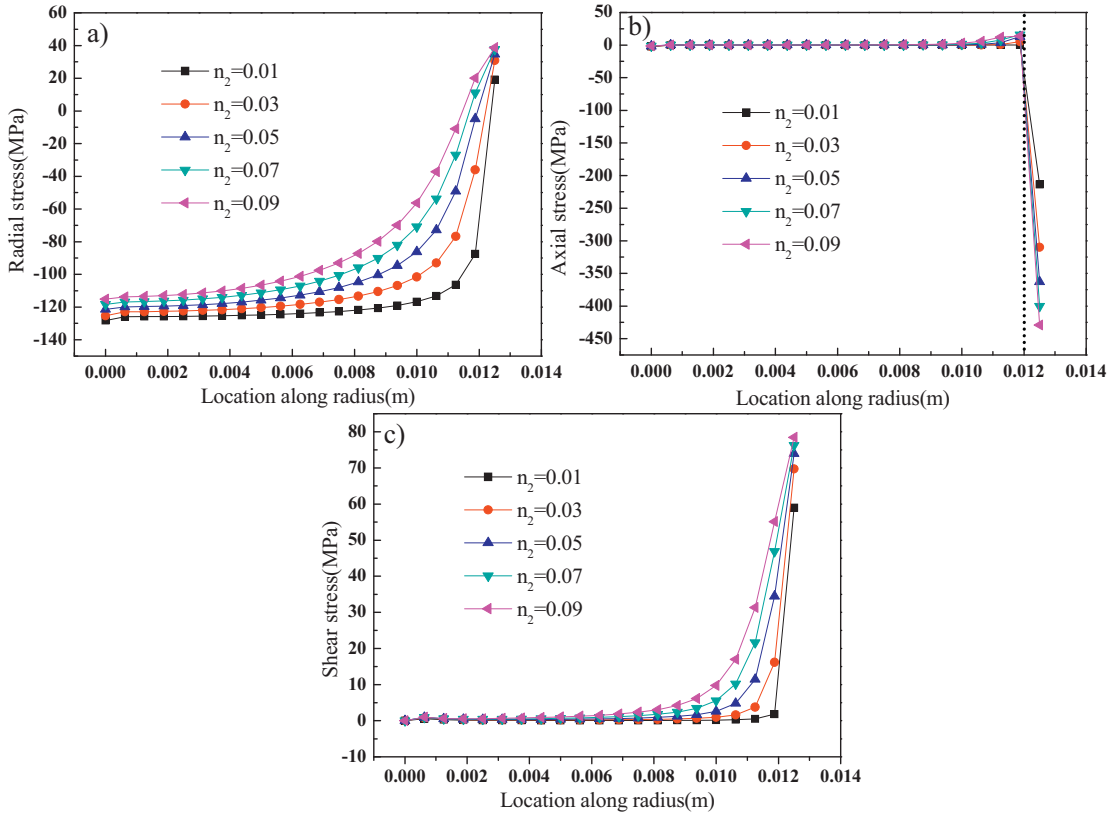

Fig. 6. Distribution of radial stress (a), axial stress (b) and shear stress (c) along the radial direction at the YSZ/BL interface with different n_2 when $n_1 = 0.02$.

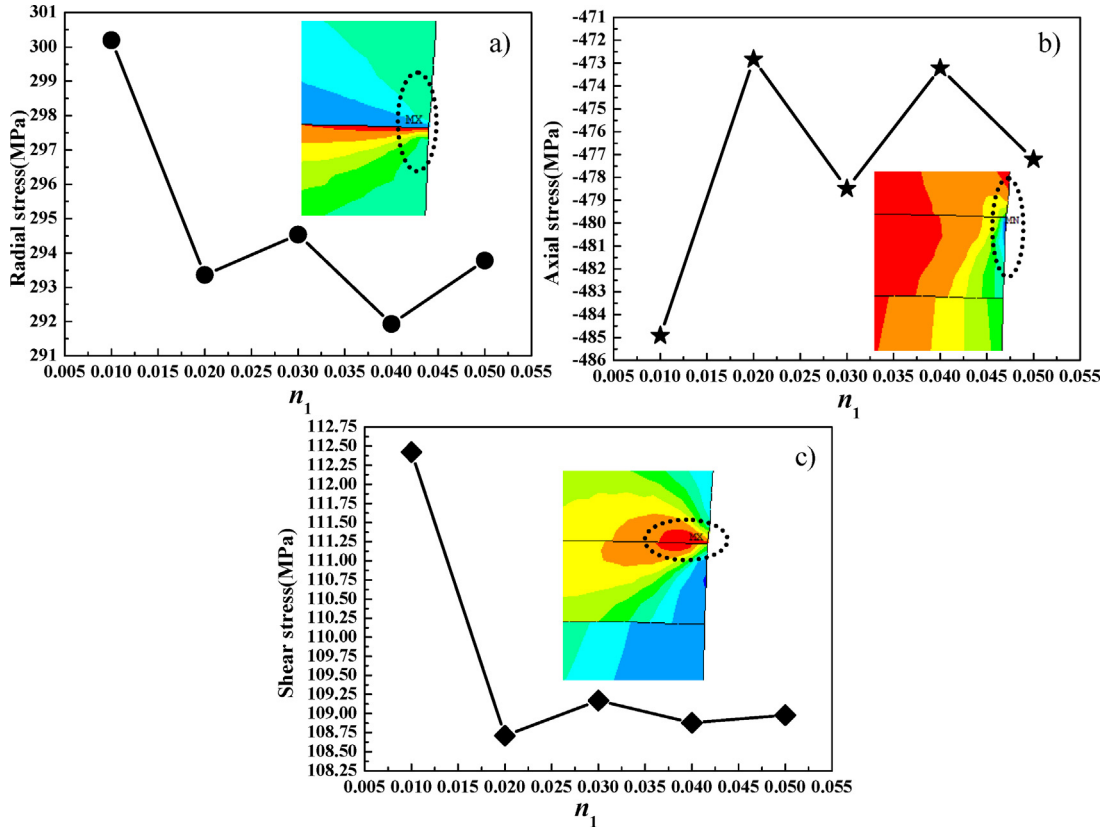

Fig. 7. Plot of radial stress, axial stress and shear stress as the function of n_1 when the double layer YSZ/BL TBCs are considered ($n_2 = 0.05$).

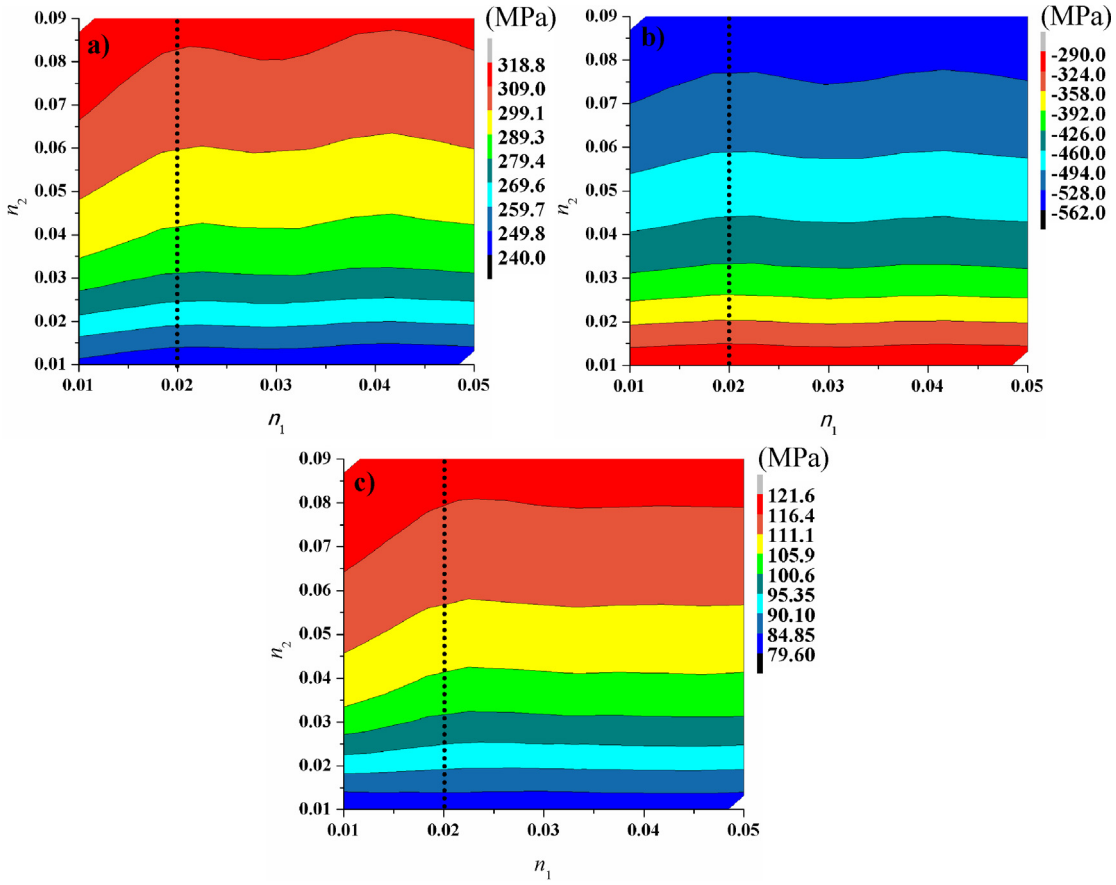

Fig. 8. The maximum radial stress (a), axial stress (b) and shear stress (c) as the function of n_1 and n_2.

and the maximum tensile stress occurs at the outer edge. Similar to the axial stress, the increase in velocity becomes higher with the increase in n_2. It can be further seen that the maximum tensile stress increases with increasing n_2 (i.e., increasing the thickness of the YSZ ceramic layer, Fig. 6c).

Fig. 7 shows the plot of radial stress, axial stress and shear stress as the function of n_1 when the double layer YSZ/BL TBC is considered ($n_2 = 0.05$). It can be seen that when n_1 is equal to 0.02, there existed minimum axial stress and shear stress. Although the radial stress did not reach the minimum value when n_1 was equal to 0.02, it still had a relatively low value. Compared with $n_1 = 0.01$, the value of the radial stress exhibited a big drop. Combined with Fig. 7a–c, it can be primarily deduced that the optimized design structure is $n_1 = 0.02$, $n_2 = 0.025$ when the double layer YSZ/BL TBC is considered. The inserted figures further show the distribution characteristic of the residual stress when $n_1 = 0.02$ and $n_2 = 0.05$. It can be further verified that the maximum radial tensile stress exists below the YSZ/BL interface near the outer edge. The maximum axial compressive stress exists at the outer edge and below the YSZ/BL interface. The maximum shear stress exists at the YSZ/BL interface near the outer edge.

In fact, the percentage of changes in maximum radial stress (s_{xx0}), axial stress (s_{yy0}) and shear stress (s_{xy0}) at the bond-coat/top-coat interface as the function of n_2 also has a very interesting changing characteristic. All the three types of residual stress increase with the increase in n_2 (i.e., increasing the thickness of the YSZ ceramic layer). In fact, the increase in the thickness of the TBC is limited. If the coating is too thick, large residual stress will be induced in the inner area of the coating and will make the coating a disastrous failure. This will further verify that the optimization results of the coating structure are $n_1 = 0.02$, $n_2 = 0.05$ for the single ceramic layer YSZ/BL TBC.

Fig. 8 shows the maximum residual stress as the function of n_1 and n_2. It can be seen that the interface lines of the three contour plots have a common characteristic. The first peak occurs at $n_1 = 0.02$; the peak indicates that higher thickness of the ceramic layer can ensure the thermal insulation capability of the TBCs, and guarantee that the residual stress has a relatively low value, such that the n_2 should be neither too high nor too low. According to the basic theory of fracture, when the residual stress reaches the yield strength (fracture strength for the ceramic material, it nearly has no plasticity and can be viewed as linear elastic), and when the residual stress exceeds the fracture strength of the YSZ ceramic layer, crack may be initiated in the inner side of the ceramic layer, and the crack may propagate, grow and eventually lead the coating to fail. Nevertheless, the plasma sprayed TBCs often have micro-pores and micro-cracks which are distributed in the ceramic layer at random, this characteristic is often attributed or determined by the feature of plasma spraying. The existence of the micro-pores and cracks can relieve the stress concentration in the inner side of the TBCs more or less and reduce the residual stress level.

3.2. Design and optimization of YSZ/IL/BL TBC

Fig. 9 shows the maximum residual stress as the function of n_2 and n_3 ($n_2 + n_3 = 0.05$). When $n_2 = 0$, $n_3 = 0.05$, only interlayer exists. Although the residual stress is very low compared with that of other cases, this is not suitable, because the thermal insulation capability

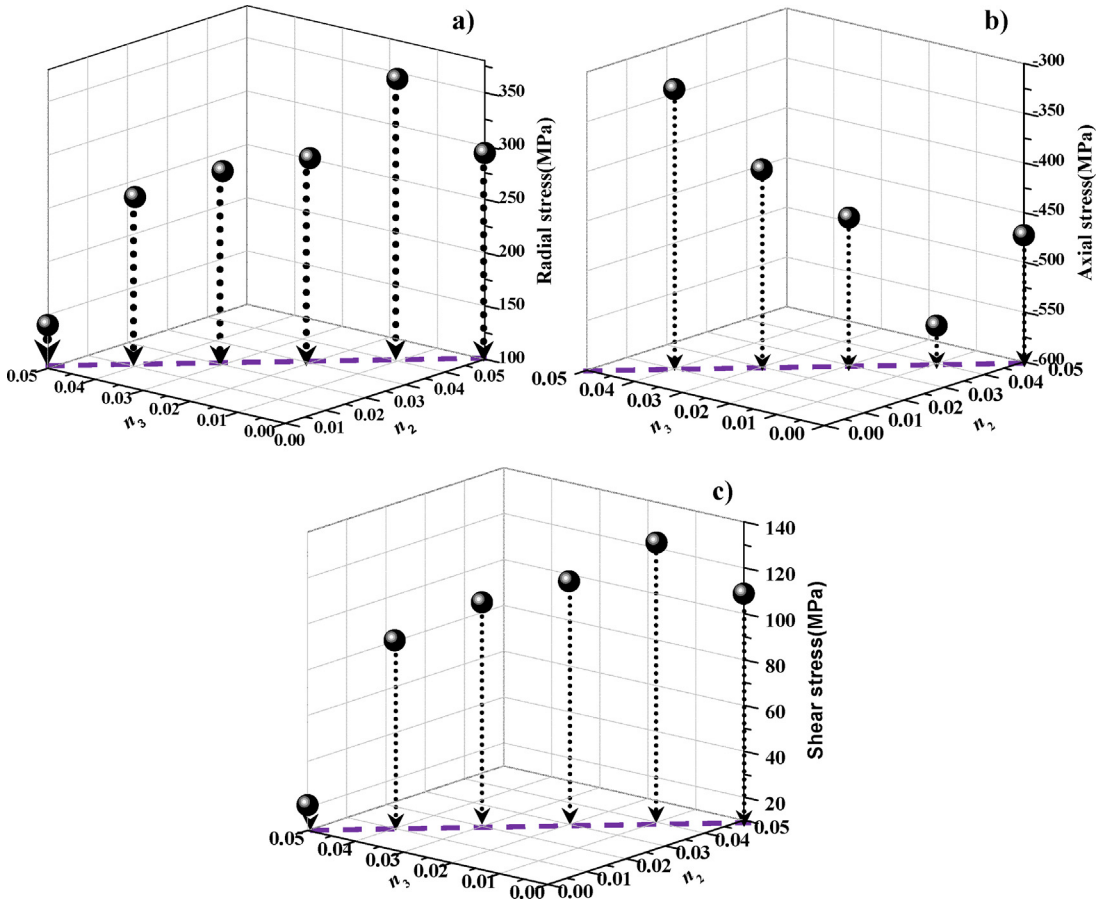

Fig. 9. The maximum radial stress (a), axial stress (b) and shear stress (c) as the function of n_2 and n_3 ($n_1 = 0.02$, $n_2 + n_3 = 0.05$).

of this type of TBCs will not be high. When $n_2 = 0.05$, $n_3 = 0$, there is no interlayer, this is just the single ceramic layer YSZ/BL TBC. It must be specifically pointed out that there existed maximum radial stress, maximum axial stress and maximum shear stress when $n_2 = 0.04$ and $n_3 = 0.01$. When both the interlayer and YSZ ceramic layer co-exists (i.e., $0 < n_2 < 0.5$, $0 < n_3 < 0.5$), the radial stress, axial stress and shear stress will decrease with the increase in n_3; this indicates that introducing the interlayer will decrease the residual stress of the TBCs and the total thickness of the TBC will remain constant. Maximum residual stress as the function of n_3 when $n_1 = 0.02$ and $n_2 = 0.05$ also showed an interesting changing characteristic. The maximum residual stress exhibited increasing tendency when n_3 was beyond 0.02, the maximum value of the maximum residual stress appeared when $n_3 = 0.1$, and the minimum value of the maximum residual stress appeared when $n_3 = 0.02$. This further verifies our prediction, which has been described earlier. In fact, the embedded layer can be designed as the functional gradient or compositional gradient coating: this is the gradient coating. The gradient coating is often composed of multilayers. Although the gradient coating can relieve stress mismatch significantly, there exists many inner interfaces, cracks can be easily initiated at these positions and the lifetime of the gradient coating is not so high. In addition, as the structure of the gradient coating is relatively complicated, the processing technique for fabricating this type of coating is not so simple and convenient. So the multilayer gradient coating is not often used in the actual application. But the gradient coating with triplex layers can still be considered and it is a very ideal coating structure. In the current discussion, it can be seen that the coating structure when $n_1 = 0.02$, $n_2 = 0.04$, $n_3 = 0.01$ is an optimized coating structure.

3.3. Design and optimization of LC/YSZ/IL/BL TBC

Fig. 10 shows the maximum residual stress as the function of n_2 and n_4 ($n_2 + n_4 = 0.05$). When $n_4 = 0.05$ and $n_2 = 0$, it can be seen that there exists maximum radial stress, axial stress and very high shear stress, this is because there is no YSZ layer when $n_4 = 0.05$ and $n_2 = 0$, only LC layer exists. As the LC layer has lower thermal expansion coefficient compared with the YSZ layer, there is more larger stress mismatch between the coating and the substrate, and the stress will also increase compared with the single ceramic layer YSZ TBC. When $n_4 = 0$ and $n_2 = 0.05$, only YSZ layer exists, this is just the single ceramic layer YSZ TBC. It has the lowest radial stress and axial stress; the shear stress is also very low. When both the YSZ layer and the LC ceramic layer co-exist (i.e., $0 < n_2 < 0.5$, $0 < n_4 < 0.5$), the axial stress will decrease with the increase in n_2; this indicates that the introduction of the LC layer will increase the maximum axial stress of the TBCs when the total thickness of the TBCs remains constant. But it does not seem to take evident effect on the radial stress and the shear stress. Considering that the LC layer has lower thermal conductivity compared with the YSZ layer, when the total thickness of the ceramic layer remains constant, the optimized structure for this type of TBCs is $n_2 = 0.04$, $n_3 = 0.01$ and $m = n_4/n_2 = 1/4$.

Fig. 11 shows the maximum residual stress as the function of n_4 when $n_1 = 0.02$, $n_2 = 0.05$ and $n_3 = 0.02$. The radial stress, axial stress and shear stress increase with increasing n_4; this will further increase when the thickness of the substrate, bond-coat layer, interlayer, YSZ layer remains the same. The residual stress will increase with increasing n_4, and the thermal insulation capability will increase with the increase in the thickness of the LC layer. The inserted figures further show the distribution characteristic of

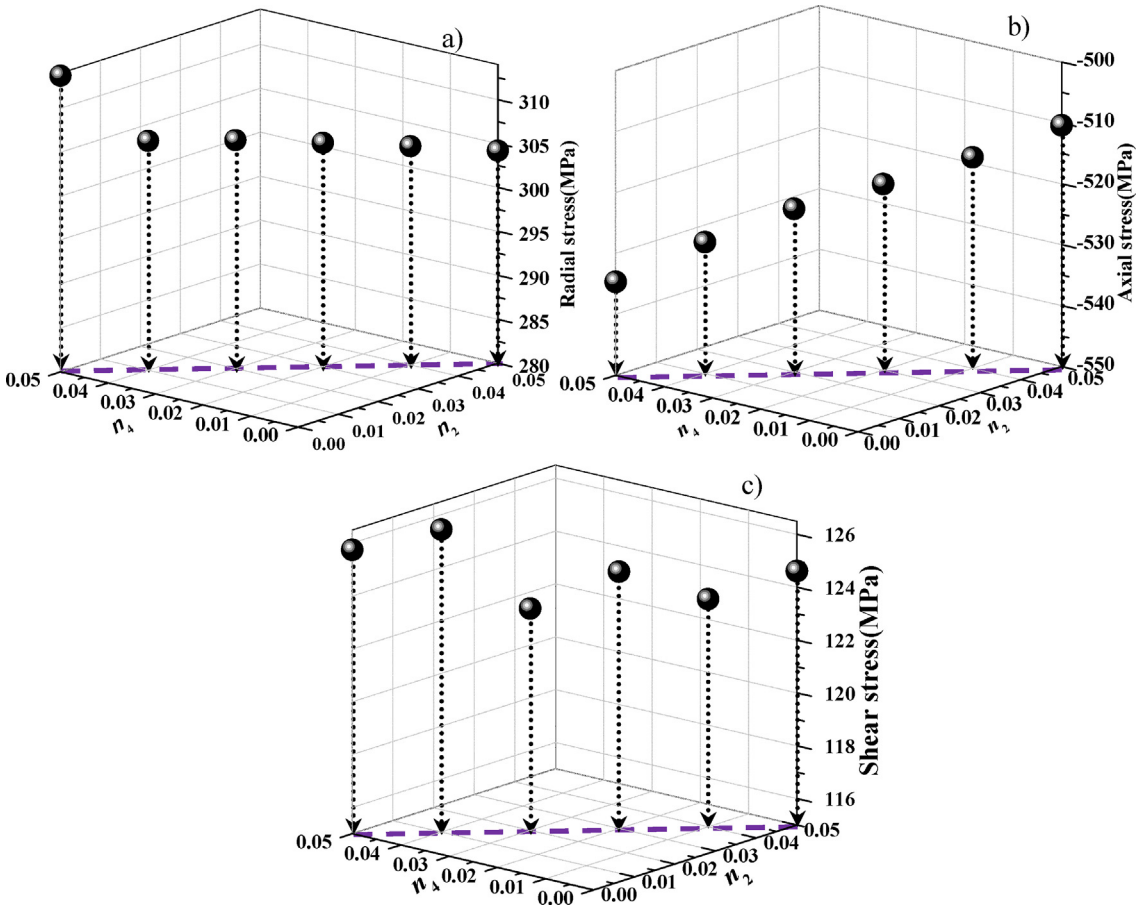

Fig. 10. The maximum radial stress (a), axial stress (b) and shear stress (c) as the function of n_2 and n_4 ($n_1 = 0.02$, $n_3 = 0.02$, $n_2 + n_4 = 0.05$).

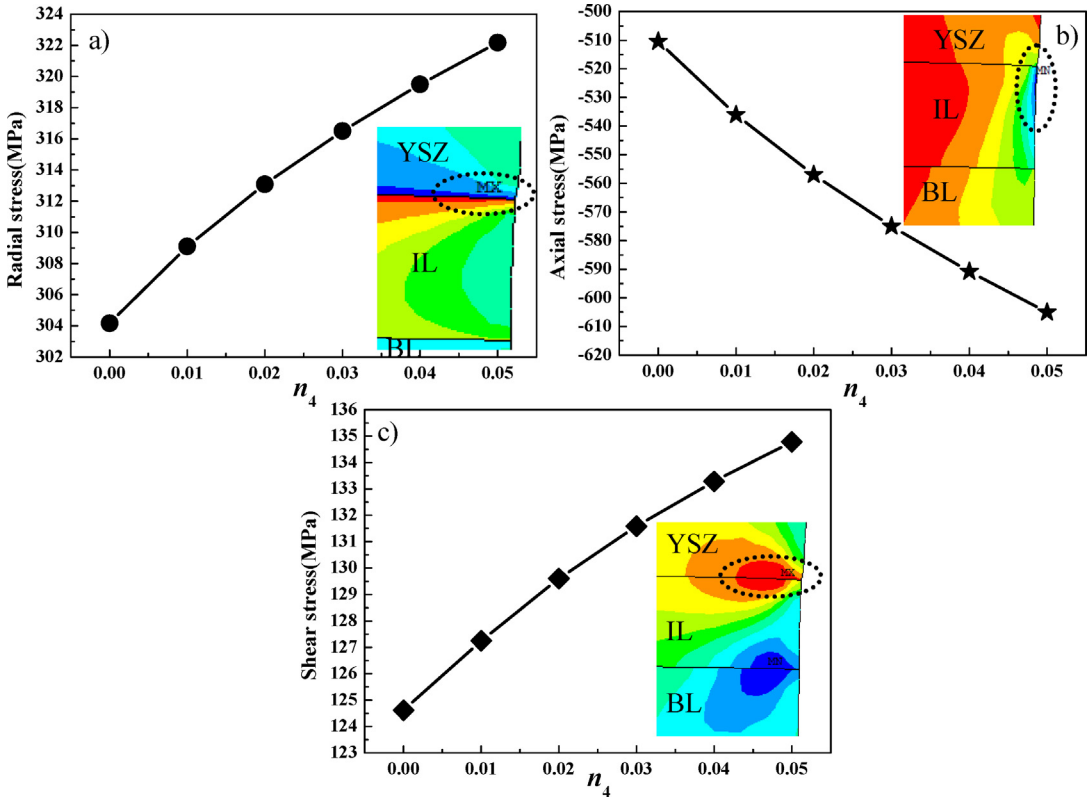

Fig. 11. The maximum radial stress (a), axial stress (b) and shear stress (c) as the function of n_4 ($n_1 = 0.02$, $n_2 = 0.05$ and $n_3 = 0.02$).

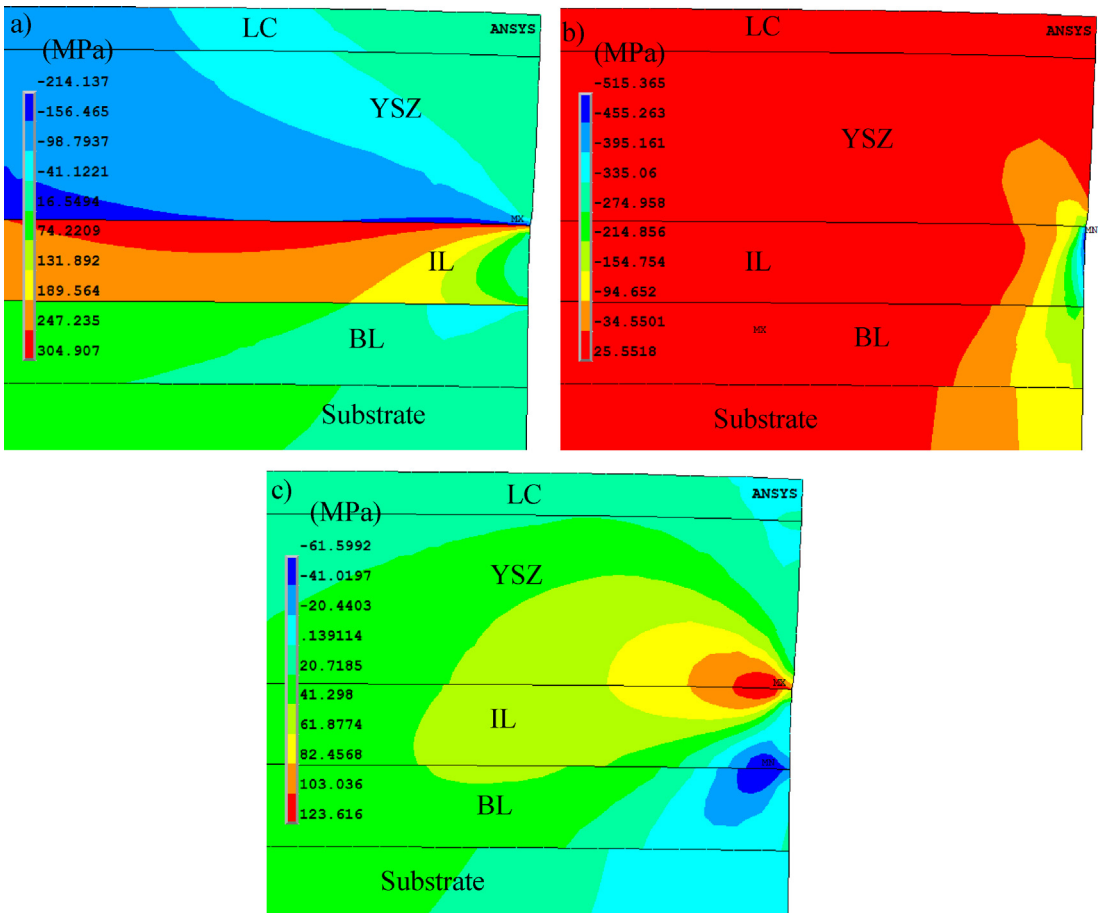

Fig. 12. Distribution of radial stress (a), axial stress (b) and shear stress (c) when $n_1 = 0.02$, $n_2 = 0.04$, $n_3 = 0.02$ and $n_4 = 0.01$.

the maximum stress. The maximum radial stress is located near the IL/YSZ interface and in the IL layer. The maximum axial stress is located at the outer edge and in the IL layer. The maximum shear stress is located at the IL/YSZ interface near the outer edge, and the board zone of the maximum shear stress is located at the YSZ layer.

Fig. 12 shows the distribution of residual stress when $n_1 = 0.02$, $n_2 = 0.04$, $n_3 = 0.02$ and $n_4 = 0.01$. It can be further verified that the maximum radial tensile stress exists below the YSZ/IL interface near the outer edge. The maximum axial compressive stress exists at the edge and below the YSZ/IL interface. Especially very interesting, the maximum tensile shear stress exists at the YSZ/IL interface near the outer edge. The maximum compressive shear stress exists at the BL/IL interface near the outer edge. The inserted figures further show the distribution characteristic of the maximum stress. Maximum radial stress is located near the IL/YSZ interface and in the IL layer. Maximum axial stress is located at the outer edge and in the IL layer. Maximum shear stress is located at the IL/YSZ interface near the outer edge, and the board zone of the maximum shear stress is located at the YSZ layer.

Fig. 13 shows the distribution of residual stress at the interface along the radial direction when $n_1 = 0.02$, $n_2 = 0.04$, $n_3 = 0.02$ and $n_4 = 0.01$. It can be seen that the radial tensile stress at the IL/BL interface firstly nearly reached a constant level, and then it exhibited an increasing tendency with the increase in the location along radius. When the location along radius exceeded a certain value (nearly $r = 0.012$ m), the tensile radial stress began to decrease with the increase in the location along radius, and it became zero when it reached the outer edge. The radial stress at the IL/YSZ interface firstly exhibited a gradual increasing tendency and then remained at a relatively low compressive stress level. When the location along the radius exceeded a certain value, the stress changed to tensile stress and exhibited increasing tendency with the increase in the location along radius. And when the location along radius exceeded $r = 0.012$ m, the stress declined and there existed minimum tensile stress at the outer edge. The shear stress at the YSZ/LC interface firstly remained at a constant compressive level, it was nearly equal to −200 MPa; when the location along radius increased, the stress began to decrease and the stress was nearly zero at the outer edge (Fig. 13a). The axial stress at the IL/BL interface, IL/YSZ interface and YSZ/LC interface firstly nearly reached zero. When the location along radius exceeded $r = 0.012$ m, the stress began to increase abruptly, and there existed maximum compressive stress at the outer edge. The maximum compressive axial stress exists at the outer edge of LC/YSZ interface (Fig. 13b). All of the three types of shear stress (the shear stress at the IL/BL interface, IL/YSZ interface and YSZ/LC interface) firstly nearly remain zero, then they have different changing tendency. The shear stress at the IL/BL interface began to increase. And when the location along radius exceeded $r = 0.012$ m, the stress began to decrease, and this stress changed from the tensile stress state to compressive stress state. The compressive stress reached the maximum value at the outer edge of the IL/BL interface, while the shear stress at the IL/YSZ interface exhibited an increasing tendency with the increasing of the location along radius. The maximum shear stress occurs at the outer edge of the IL/YSZ interface. The shear stress at the YSZ/LC interface remains at a relatively low level (Fig. 13c).

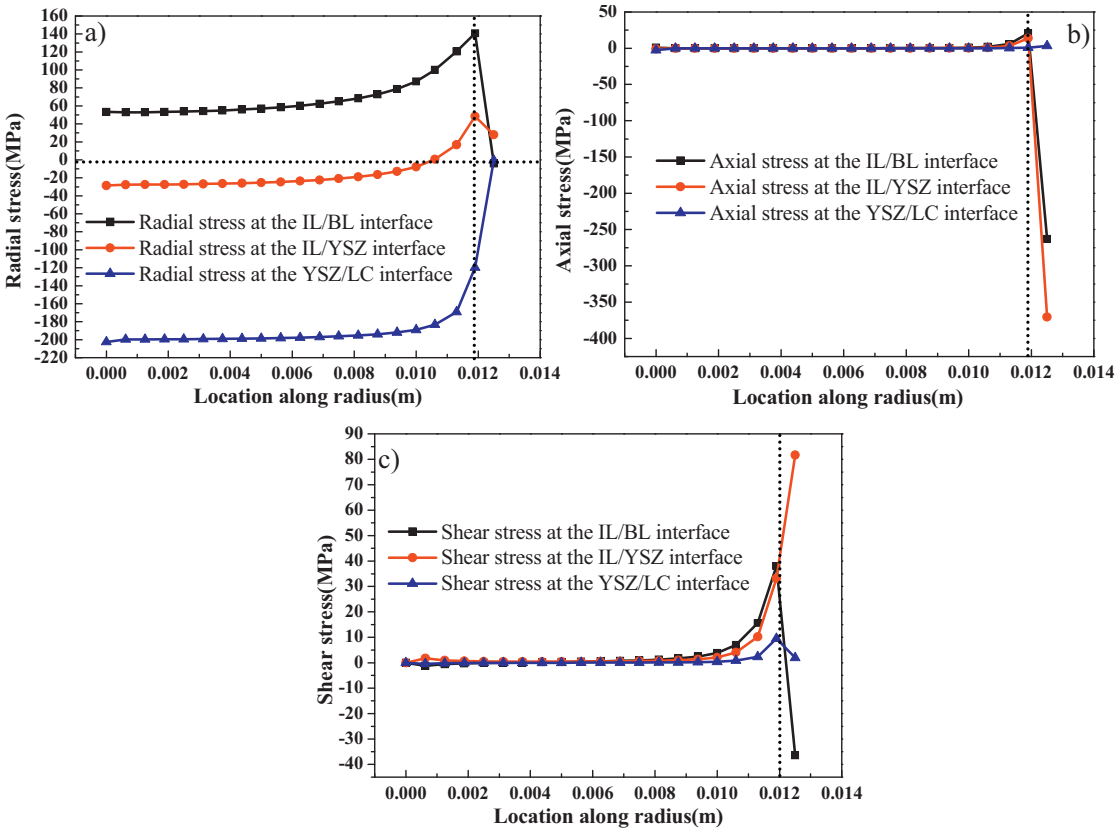

Fig. 13. Distribution of radial stress (a), axial stress (b) and shear stress (c) along the radial direction when $n_1 = 0.02$, $n_2 = 0.04$, $n_3 = 0.02$ and $n_4 = 0.01$.

The typical failure patterns of this optimized LC/YSZ/IL/BL coating structure can be described as follows: the maximum radial stress often occurred at the IL/BL interface and near to the coating edge, while both the maximum axial stress and shear stress often occurred at the outer edge of the IL/YSZ interface. This kind of coating will produce failure at these positions. The maximum radial stress will promote the coating delaminate along the IL/BL interface. The maximum axial stress and shear stress will make the coating buck at the outer edge of the IL/YSZ interface.

3.4. Optimization of the TBCs from the aspect of thermal insulation effect

Fig. 14 shows the contour map of the temperature distribution of YSZ/BL, YSZ/IL/BL and LC/YSZ/IL/BL TBCs. It can be seen that when the coating surface temperature is constant, the LC/YSZ/IL/BL TBCs have the highest thermal insulation temperature, and the temperature distribution of all the three types of TBCs exhibited layer-like characteristic, which is more evident in the ceramic layer. This is because all the interfaces in all the three types of TBCs are flat and no defects were introduced in the finite element model. In fact, the amount of pores and cracks that are distributed at random exists in the plasma-sprayed TBCs (especially the horizontal cracks that are vertical to the through-thickness direction) will play an important role in reducing the effective thermal conductivity of the as-sprayed TBCs. But these factors are not considered in the current work as we focused on the design and optimization of the layer structure.

Fig. 15 shows the plot of temperature distribution and effective thermal conductivity of YSZ/BL, YSZ/IL/BL and LC/YSZ/IL/BL TBCs when the surface temperature equals 1473 K. It can be seen that all the three types of TBCs have a high temperature gradient along the thorough-thickness direction of the ceramic layer; the LC/YSZ/IL/BL TBC has the highest thermal insulation temperature ($\Delta T_1 > \Delta T_2 > \Delta T_3$). The calculated effective thermal conductivities are also displayed in the inserted figure. The effective thermal conductivities of the YSZ/BL, YSZ/IL/BL and LC/YSZ/IL/BL TBC are 1.44 W/m K, 1.32 W/m K and 1.25 W/m K, respectively. It can be seen that the LC/YSZ/IL/BL has the lowest effective thermal conductivity. The effective thermal conductivity of these optimized TBCs is 13.2% lower than that of the typical single ceramic layer YSZ/BL TBC.

Based on the above discussion, the optimized coating structure is the LC/YSZ/IL/BL TBC, and the corresponding values of the optimized parameters are $n_1 = 0.02$, $n_2 = 0.04$, $n_3 = 0.02$ and $n_4 = 0.01$ ($m = 0.25$). The optimized results agreed well with Dai and Cao's work [61,5]. In addition, according to our previous published work, the double ceramic layer TBCs usually have higher thermal shock resistance and higher high temperature oxidation resistance ability, which further confirm that the structure optimization of the APS-TBCs plays an important role in improving the performance of the as-sprayed TBCs [62].

3.5. Experimental verification

The experimental process was performed in order to further verify our results of design and optimization. The detailed

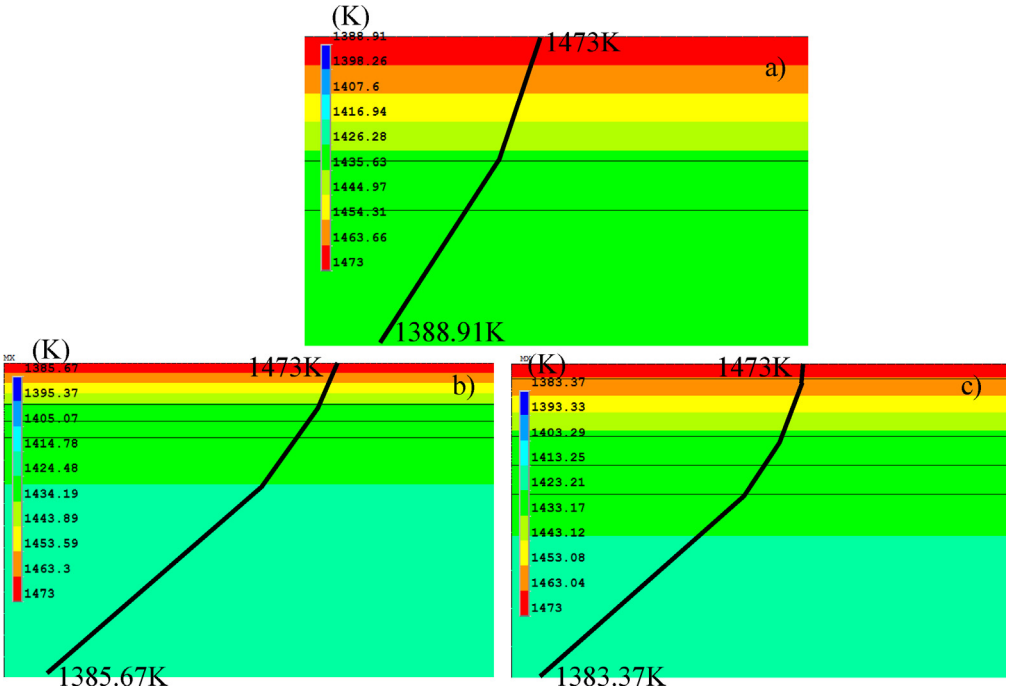

Fig. 14. Contour map of temperature distribution of YSZ/BL, YSZ/IL/BL and LC/YSZ/IL/BL TBC.

experimental procedure can be also seen in our previous work [63]. Indeed, the thickness of the as-sprayed coating is an important factor, but previous research indicate that when the thickness exceeds a certain value, the residual stress will increase slightly with the increase in thickness [64,65], and the change in thickness will not change the actual positions of the maximum residual stress, which can be also seen in our current work; therefore, the difference in thickness is not a focused problem. In addition, according to the basic theory, residual stress plays an important role in affecting the thermal shock life of the as-sprayed TBC. Usually, the large residual stress can lead to a short thermal cycle life; this is because that the maximum stress often exists near the metallic layer/ceramic layer interface at the outer edge, and the failure position of the TBCs after thermal shock is often located at or near these positions. It is therefore reasonable to evaluate the thermal shock behavior based on the distribution of the residual stress field of the as-sprayed TBCs.

It is generally believed that thermal shock resistance of ceramics can be characterized by thermal shock factors R and R'. As shown in the following formula, thermal shock resistance of a ceramic coating depends on the thermal expansion coefficient, elastic modulus and thermal conductivity coefficient [26,66]:

$$R = \frac{\sigma_c}{\alpha E}(B_i \gg 1) \tag{12}$$

$$R' = \frac{\sigma_c \lambda}{\alpha E} = Rk(B_i \ll 1) \tag{13}$$

where α is the thermal expansion coefficient, E is the effective elastic modulus, k is the thermal conductivity, σ_c is denoted as the stress distributed in the ceramic coating and B_i is Biot number:

$$B_i = \frac{hL}{k} \tag{14}$$

where h is the (constant) heat transfer coefficient and L is the length of the body. It can be seen from these expressions, the thermal shock resistance is dependent on the residual stress and is proportional to the residual stress. So it is beneficial to improve the thermal shock resistance of the as-sprayed TBC from the aspect of reducing the residual stress. Based on the above discussion, it can be further predicated that the thermal shock resistance ability of the as-sprayed TBC can be used to evaluate and examine the optimized coating structure. Fig. 16 shows the cross-section image of the as-sprayed single ceramic layer YSZ TBCs and double ceramic layer LC/YSZ TBCs. As for the single ceramic layer YSZ TBCs, it can be seen that the coating began to fail after enduring a high temperature thermal shock with the thermal cycle number equal to 19. The failure mechanism can be explained as follows: a vertical crack originated from the surface propagated toward the interface between the bond-coat and top-coat; the horizontal crack initiated, grew and propagated along the interface direction and then the delamination occurred. The thin thermally grown oxide (TGO) layer can be also seen at the YSZ/NiCoCrAlY interface. However under the same condition, the double ceramic layer LC/YSZ

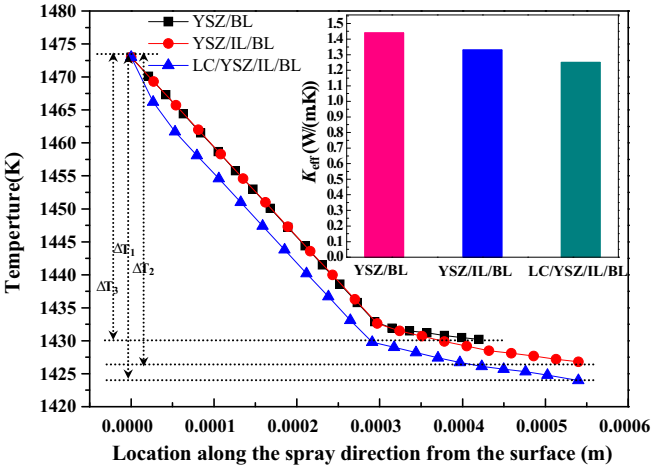

Fig. 15. Plot of temperature distribution and effective thermal conductivity of YSZ/BL, YSZ/IL/BL and LC/YSZ/IL/BL TBCs when the surface temperature equals 1473 K.

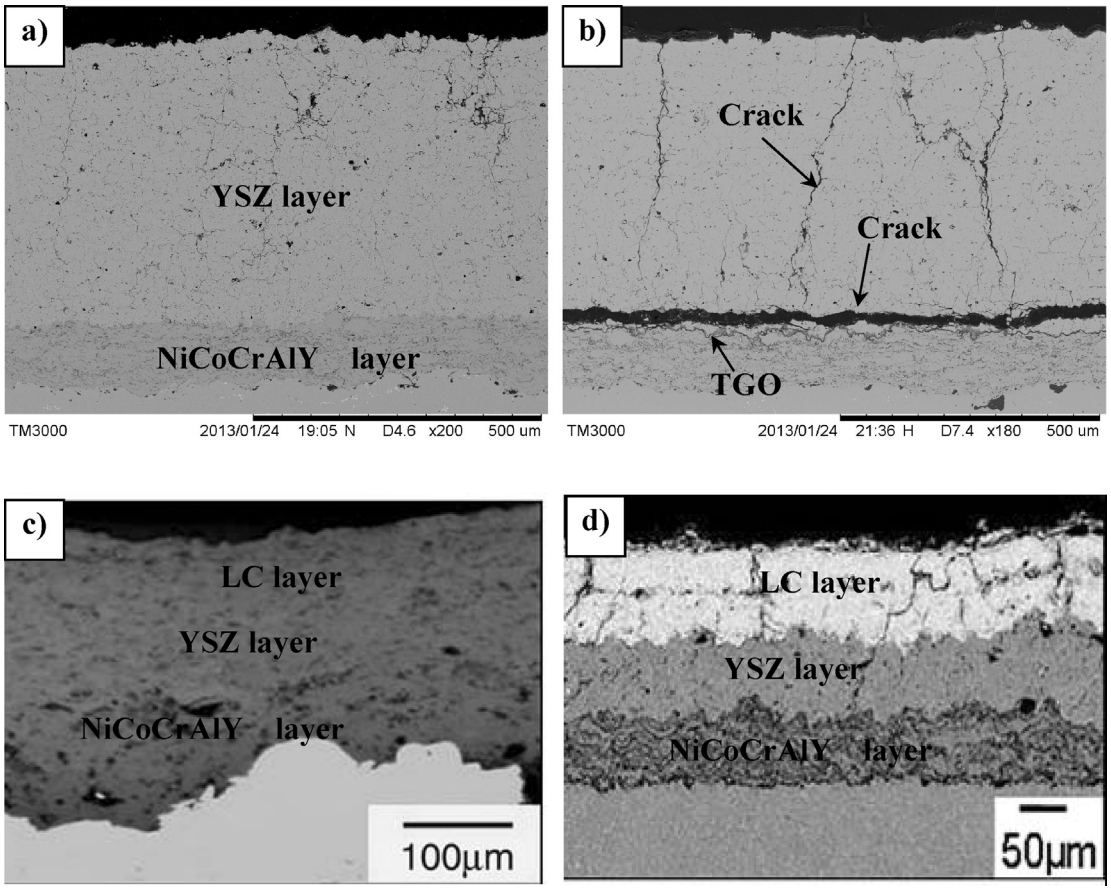

Fig. 16. Cross-section image of the as-sprayed single ceramic layer YSZ TBC and double ceramic layer LC/YSZ TBC: (a) as-sprayed YSZ TBC, (b) YSZ TBC after thermal shock with the thermal cycle number equal to 19, (c) as-sprayed LC/YSZ TBC, and (d) LC/YSZ TBC after thermal shock with thermal cycle number equal to 2100 [67].

did not show evident failure trace after high temperature thermal shock with the thermal cycle number equal to 2100. This further shows that the double ceramic layer TBCs have significant advantage compared with the single ceramic layer TBCs. And it further reflects that the coating structure with double ceramic layer is a very good selection. It has an excellent match between the low residual stress and high thermal insulation: both these factors will promote the enhancement of the thermal shock resistance ability of the optimized coating.

As the property parameters used in the current work may not reflect the actual coatings, the design and optimization results may have some difference from the actual cases. But the current work will provide a powerful guide to design the TBCs with excellent performance (low residual stress and high thermal insulation effect). In fact, the property parameters can be measured using the experimental method, the design and optimization results can be obtained using the measured parameters, but the methods using in the current work have paved a path for designing various types of TBCs with complicated structure. The TBCs with long lifetime, high reliability and durability can be fabricated based on the design and optimization results; so it is of great significance to perform the process of materials design before the fabrication of materials.

4. Conclusions

The design and optimization of the coating structure for APS-TBC were performed by finite element simulation in the current work. And the stress distribution of different types of TBCs considering the thermal insulation effect simultaneously has been discussed. The corresponding conclusions can be drawn:

(1) The bond-coat layer and interlayer only take an effect on relieving the stress mismatch, the layers cannot be too thick. The suitable thickness scope of the bond-coat is in the range of 60–120 μm. The zirconate-based layer alone cannot be used as the thermal barrier layer in a single ceramic layer, it must be combined with the YSZ ceramic layer.
(2) The thickness ratio between the zirconate layer and the YSZ layer is usually lower than 1, and the zirconate-based layer is often deposited onto the surface of the YSZ layer. The optimized thickness ratio between the LC layer and YSZ layer is 1/4.
(3) The optimized coating structure is $n_1 = 0.02$, $n_2 = 0.04$, $n_3 = 0.02$ and $n_4 = 0.01$. In our current simulation work, when the thickness of the substrate is 6 mm, the thickness of the bond-coat, YSZ layer, interlayer, and LC layer is 120 μm, 240 μm, 120 μm and 60 μm, respectively.
(4) As for the optimized LC/YSZ/IL/BL coating structure, the maximum radial stress often occurs at the IL/BL interface and near to the outer edge of the coating, while both the maximum axial stress and shear stress often occur at the outer edge of IL/YSZ interface. This kind of coating will fail at these positions. The maximum radial stress will promote the coating delaminate along the IL/BL interface. The maximum axial stress and shear stress will make the coating buck at the outer edge of the IL/YSZ interface.
(5) As the double ceramic layer has a significant advantage, due to the residual stress mismatch and thermal insulation effect,

compared with the single ceramic layer YSZ TBC, the double ceramic layer TBCs may be an important direction for the advanced TBCs in the future.

Acknowledgements

We express our gratitude to the high Speed Computational Center of Harbin Institute of Technology (HIT) for providing software support. We also thank Dr. Yuexing Zhao for providing some experimental data to verify our simulation results. This work was jointly supported by the National Natural Science Foundation of China (NSFC) under the Grant No. 51202277, Young Scholar Project (No. 12ZR1452000) supported by the Shanghai Science and Technology Committee, and 2012 Innovation Fund of SICCAS (Y35ZC6160G). We also appreciate Prof. Chuanxian Ding for his useful advices and comments on our article.

References

[1] P.P. Nitin, G. Maurice and H.J. Eric, Science, 296, 279–284 (2002).
[2] A.G. Evans, D.R. Mumm, J.W. Hutehinson, G.H. Meier and F.S. Pettit, Prog. Mater. Sci., 46, 505–553 (2001).
[3] M. Ranjbar-far, J. Absi, G. Mariaux and D.S. Smith, Mater. Des., 32, 4961–4969 (2011).
[4] S. Uwe, L. Christoph, F. Klaus, P. Manfred, S.B. Bilge, L. Odile et al., Aerosp. Sci. Technol., 7, 73–80 (2003).
[5] X.Q. Cao, R. Vassen, F. Tietz and D. Stöver, J. Eur. Ceram. Soc., 26, 247–251 (2006).
[6] H.F. Liu, S.L. Li, Q.L. Li and Y.M. Li, Mater. Des., 31, 2972–2977 (2010).
[7] A. Rabieia and A.G. Evans, Acta Mater., 48, 3963–3976 (2000).
[8] M. Gupta, N. Curry, P. Nylén, N. Markocsan and R. Vaßen, Surf. Coat. Technol., 220, 20–26 (2013).
[9] M. Abbasa, L. Guo and H.B. Guo, Ceram. Int., 39, 5103–5111 (2013).
[10] S. Kyaw, A. Jones and T. Hyde, Eng. Fail. Anal., 27, 150–164 (2013).
[11] X.S. Yang, J. Wan, C.Y. Dai, Y. Zhang, W.G. Mao, Y.C. Zhou and C. Lu, Surf. Coat. Technol., 223, 87–91 (2013).
[12] K. Al-Athel, K. Loeffel, H.W. Liu and L. Anand, Surf. Coat. Technol., 222, 68–78 (2013).
[13] J.H. Qiao, R. Bolot and H.L. Liao, Surf. Coat. Technol., 220, 170–173 (2013).
[14] P. Seiler, M. Baker and J. Rosler, Comput. Mater. Sci., 80, 27–34 (2013).
[15] J. Wu, X.Z. Wei, N.P. Padture, P.G. Klemens, M. Gell, E. García, P. Miranzo and M.I. Osendi, J. Am. Ceram. Soc., 85, 3031–3035 (2002).
[16] Z. Wang, A. Kulkarni, S. Deshpande, T. Nakamura and H. Herman, Acta Mater., 51, 5319–5334 (2003).
[17] I.O. Golosnoy, S.A. Tsipas and T.W. Clyne, J. Therm. Spray Technol., 14, 205–214 (2005).
[18] A.K. Raya, S.C. Bosea, P.K. Dea and D.K. Das, Mater. Sci. Eng. A, 527, 5474–5483 (2010).
[19] C. Giolli, A. Scrivani, G. Rizzi, F. Borgioli, G. Bolelli and L. Lusvarghi, J. Therm. Spray Technol., 18, 223–230 (2009).
[20] G. Lim and A. Kar, J. Phys. D: Appl. Phys., 42, 155412 (2009).
[21] G. Lee, A. Atkinson and A. Selçuk, Surf. Coat. Technol., 201, 3931–3936 (2006).
[22] W.G. Mao, Y.C. Zhou, L. Yang and X.H. Yu, Mech. Mater., 38, 1118–1127 (2006).
[23] L. Wang, Y. Wang, X.G. Sun, Z.Y. Pan, J.Q. He and C.G. Li, Appl. Surf. Sci., 257, 2238–2249 (2011).
[24] F. Sen, O. Sayman, M. Toparli and E. Celik, J. Mater. Process. Technol., 180, 239–245 (2006).
[25] M. Ranjbar-Far, J. Absi, S. Shahidi and G. Mariaux, Mater. Des., 32, 728–735 (2011).
[26] O. Sarikaya, Y. Islamoglu and E. Celik, Mater. Des., 26, 357–362 (2005).
[27] H.J. Rätzer-Scheibe, U. Schulc and T. Krell, Surf. Coat. Technol., 200, 5636–5644 (2006).
[28] F. Cernuschia, S. Ahmaniemi, P. Vuoristoc and T. Mantyla, J. Eur. Ceram. Soc., 24, 2657–2667 (2004).
[29] X.C. Zhang, B.S. Xu, H.D. Wang and Y.X. Wu, Thin Solid Films, 488, 274–282 (2005).
[30] L. Wang, Y. Wang, X.G. Sun, Z.Y. Pan, J.Q. He, Y. Zhou and P.L. Wu, Surf. Interface Anal., 43, 869–880 (2011).
[31] H.B. Guo, R. Vaßen and D. Stöver, Surf. Coat. Technol., 186, 353–363 (2004).
[32] M. Karger, R. Vaßen and D. Stöver, Surf. Coat. Technol., 206, 16–23 (2011).
[33] H.B. Guo, H. Murakami and S. Kuroda, J. Am. Ceram. Soc., 89, 3797–3804 (2006).
[34] H.B. Guo, H. Murakami and S. Kuroda, Mater. Trans., 46, 1775–1778 (2005).
[35] P.H. Lee, S.Y. Lee, J.Y. Kwon, S.W. Myoung, J.H. Lee, Y.G. Jung, H. Cho and U. Paik, Surf. Coat. Technol., 205, 1250–1255 (2010).
[36] Y. Wang, W. Tian, Y. Yang, C.G. Li and L. Wang, Mater. Sci. Eng. A, 516, 103–110 (2009).
[37] S. Widjaja, A.M. Limarga and T.H. Yip, Thin Solid Films, 434, 216–227 (2003).
[38] L. Wang, Y. Wang, X.G. Sun, J.Q. He, Z.Y. Pan and C.H. Wang, Comput. Mater. Sci., 53, 117–127 (2012).
[39] P. Chris, I. Jan, W. Hsin, P. Wally and T. Rodney, Surf. Coat. Technol., 205, 57–65 (2010).
[40] C.A. Andersson, J. Greggi, T.K. Gupta, N. Claussen, M. Ruhle and A.H. Heuer, Science and Technology of Zirconia II, Advances in Ceramics, vol. 12, The American Ceramic Society, Columbus, OH (1984), pp. 78–85.
[41] G. Witz, V. Shklover and W. Steurer, J. Am. Ceram. Soc., 90, 2935–2940 (2007).
[42] J. Chevalier and L. Gremillardw, J. Am. Ceram. Soc., 92, 1901–1920 (2009).
[43] P. Scardi, M. Leoni and L. Bertamini, Surf. Coat. Technol., 76–77, 106–112 (1995).
[44] J. Moon, H. Choi, H. Kim and C. Lee, Surf. Coat. Technol., 155, 1–10 (2002).
[45] R. Vaßen, M.O. Jarligo, T. Steinke, D.E. Mack and D. Stöver, Surf. Coat. Technol., 205, 938–942 (2010).
[46] X.Q. Cao, R. Vassen, W. Fischer, F. Tietz, W. Jungen and D. Stöver, Adv. Mater., 15, 1438–1442 (2003).
[47] K. Kokini, J. DeJonge, S. Rangaraj and B. Beardsley, Surf. Coat. Technol., 154, 223–231 (2002).
[48] X.C. Zhang, B.S. Xu, H.D. Wang, Y.X. Wu and Y. Jiang, Mater. Des., 28, 1192–1197 (2007).
[49] K.A. Khor and Y.W. Gu, Mater. Sci. Eng. A, 277, 64–76 (2000).
[50] J.D. Lee, H.Y. Ra, C.T. Hong and S.K. Hur, Surf. Coat. Technol., 56, 27–37 (1992).
[51] S.C. Joshi and H.W. Ng, Simul. Model. Pract. Th., 19, 586–598 (2011).
[52] ANSYS Inc. Release13.0. Documentation for ANSYS.
[53] X.C. Zhang, B.S. Xu, H.D. Wang and Y.X. Wu, Mater. Des., 27, 308–315 (2006).
[54] Z. Gan, H.W. Ng and A. Devasenapathi, Surf. Coat. Technol., 187, 307–319 (2004).
[55] H.W. Ng and Z. Gan, Finite Elem. Anal. Des., 41, 1235–1254 (2005).
[56] V. Teixeira, M. Andritschky, W. Fischer, H.P. Buchkremer and D. Stöver, Surf. Coat. Technol., 120–121, 103–111 (1999).
[57] R.E. Taylor, Mater. Sci. Eng. A, 245, 160–167 (1998).
[58] P. Michlik and C. Berndt, Surf. Coat. Technol., 201, 2369–2380 (2006).
[59] L. Wang, Y. Wang, X.G. Sun, Z.Y. Pan, J.Q. He, Y. Zhou and P.L. Wu, Mater. Des., 32, 36–47 (2011).
[60] L. Wang, Y. Wang, X.G. Sun, J.Q. He, Z.Y. Pan and C.H. Wang, Mater. Des., 35, 505–517 (2012).
[61] P. Michlik and C. Berndt, Surf. Coat. Technol., 206, 2369–2380 (2001).
[62] L. Wang, Y. Wang and X.G. Sun, Mater. Sci. Forum, 49, 617–632 (2013).
[63] L. Wang, Y. Wang, X.G. Sun, J.Q. He, Z.Y. Pan and C.H. Wang, Ceram. Int., 38, 3595–3606 (2012).
[64] C.M. Weyant, J. Almer and K.T. Faber, Acta Mater., 58, 943–951 (2010).
[65] L.J. Gu, X.Z. Fan, Y. Zhao, B.L. Zou, Y. Wang, S.M. Zhao and X.Q. Cao, Surf. Coat. Technol., 206, 4403–4410 (2012).
[66] G.A. Schneider, World Ceramics Congress, Florence, Italy, (1990) pp. 24–30.
[67] H.B. Guo, Y. Wang, L. Wang and S.K. Gong, J. Therm. Spray Technol., 18, 665–671 (2009).